


Review

# A Novel Non-Destructive Technique for Cultural Heritage: Depth Profiling and Elemental Analysis Underneath the Surface with Negative Muons

Matteo Cataldo <sup>1,2,3,\*</sup> , Massimiliano Clemenza <sup>1,2</sup>, Katsuiko Ishida <sup>4</sup> and Adrian D. Hillier <sup>3</sup> 

<sup>1</sup> Dipartimento di Fisica “Giuseppe Occhialini”, Università Degli Studi di Milano Bicocca, 20126 Milano, Italy; massimiliano.clemenza@mib.infn.it

<sup>2</sup> INFN Sezione Milano Bicocca, 20126 Milano, Italy

<sup>3</sup> ISIS Neutron and Muon Source, STFC Rutherford Appleton Laboratory, Didcot OX11 0QX, UK; adrian.hillier@stfc.ac.uk

<sup>4</sup> RIKEN, Wako 351-0198, Japan; ishida@riken.jp

\* Correspondence: m.cataldo6@campus.unimib.it; Tel.: +39-3463-018-395

**Abstract:** Scientists, curators, historians and archaeologists are always looking for new techniques for the study of archaeological artefacts, especially if they are non-destructive. With most non-destructive investigations, it is challenging to measure beneath the surface. Among the vast board of techniques used for cultural heritage studies, it is difficult to find one able to give information about the bulk and the compositional variations, along with the depth. In addition, most other techniques have self-absorption issues (i.e., only surface sensitive) and limited sensitivity to low Z atoms. In recent years, more and more interest has been growing around large-scale facility-based techniques, thanks to the possibility of adding new and different insights to the study of material in a non-destructive way. Among them, muonic X-ray spectroscopy is a very powerful technique for material characterization. By using negative muons, scientists are able to perform elemental characterization and depth profile studies. In this work, we give an overview of the technique and review the latest applications in the field of cultural heritage.

**Keywords:** muonic X-ray; muonic atoms; muon spectroscopy; elemental analysis; depth profiling; archaeometry



**Citation:** Cataldo, M.; Clemenza, M.; Ishida, K.; Hillier, A.D. A Novel Non-Destructive Technique for Cultural Heritage: Depth Profiling and Elemental Analysis Underneath the Surface with Negative Muons. *Appl. Sci.* **2022**, *12*, 4237. <https://doi.org/10.3390/app12094237>

Academic Editor: Giuseppe Lacidogna

Received: 30 March 2022

Accepted: 20 April 2022

Published: 22 April 2022

**Publisher's Note:** MDPI stays neutral with regard to jurisdictional claims in published maps and institutional affiliations.



**Copyright:** © 2022 by the authors. Licensee MDPI, Basel, Switzerland. This article is an open access article distributed under the terms and conditions of the Creative Commons Attribution (CC BY) license (<https://creativecommons.org/licenses/by/4.0/>).

## 1. Introduction

Non-destructive elemental analysis is a fundamental step in the study of an archaeological artefact. By knowing the composition of a material, scientists, historians, and curators can make assumptions about the manufacturing process of an object, investigate the origins of the material or infer information about the historical context of populations. Nowadays, many techniques can provide such information: X-ray fluorescence (XRF), scanning electron microscopy (SEM), particle-induced X-ray emission (PIXE) or mass spectroscopy (MS) [1–4]. However, some of these techniques (XRF, PIXE and SEM) have problems in overcoming the alteration patinas that could be present in freshly excavated or corroded samples, and some of them (SEM and MS) are invasive and destructive techniques. In archaeological metals and metal alloys, especially, alteration phases are quite common, not only on the surface of the sample but also in the first layers of the material. However, the above-mentioned techniques are only surface and near-surface methods, and no information from the core of the material is acquired. On the other hand, bulk analysis with neutron-based techniques [5], due to their high penetration depth, do not give information about the surface and the first layers of the investigated material. Depth profiling is possible for other types of samples, such as paintings (here, however, we omit discussion, but recommend [6]). Therefore, it is critical to have a technique that provides

information both from the surface and from the core of a sample. In recent years, a new tool for non-destructive surface and bulk analysis is represented by Muonic Atom X-ray Emission Spectroscopy ( $\mu$ -XES) [7]. The basis of  $\mu$ -XES is similar to X-ray fluorescence: it relies on the interaction between a fundamental particle—the negative muon—and a capturing material and the detection of the following X-ray emission. Given that the muon mass is about 200 times bigger than the electron, the emitted X-rays are highly energetic. This allows overcoming problems of self-absorption of common techniques, such as XRF or PIXE, and makes low  $Z$  atoms detectable. For example, the  $K\alpha$  transition energy for muonic lithium ( $Z = 3$ ) is 19 keV [8], which corresponds to the energy of the  $K\alpha$  of rhodium ( $Z = 45$ ) in conventional X-ray fluorescence. Furthermore, as mentioned above, the muon is bigger than the electron but smaller than the proton—this mass difference corresponds to a less effective bremsstrahlung effect (compared to electrons) and a deeper penetration depth (compared to protons), thus making bulk analysis feasible. Finally, by varying the energy of the incident muon beam, it is possible to vary the penetration depth and select the position of the analysis. For these reasons, muonic atom X-ray spectroscopy represents an invaluable tool for elemental analysis; owing to the high penetration depth and negligible self-absorption effects, it can overcome the problems of the aforementioned techniques and give new insights into the study of an archaeological artefact. In this paper, we give an overview of the technique and review the latest applications in the field of cultural heritage.

## 2. Muons

### 2.1. Properties of the Muon and Muon Capture

Muons are elementary particles (leptons) identified by the Greek letter “ $\mu$ ” that can be positively or negatively charged. With a mass that is almost 207 times the mass of the electron, a negative muon is considered a “heavy electron”, with an electric charge of  $-1$  and  $1/2$  spin. As an unstable particle, the muon has a mean lifetime of  $2.2 \mu\text{s}$ . The negative muon, other than the decay process, can experience capture by an atom, giving rise to the so-called “muonic atom” (Figure 1): the time scale of this process is in the order of  $10^{-13}$  s.

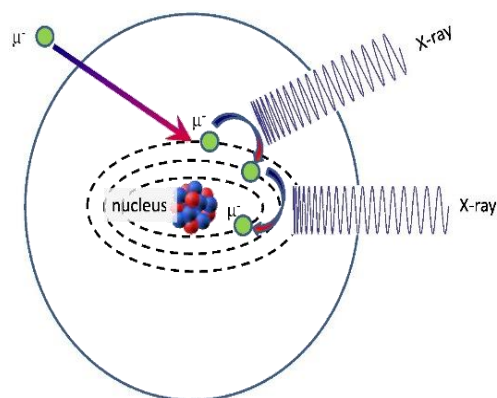


**Figure 1.** Muonic capture process. The muon then has a finite probability of being captured by the nucleus and may emit a gamma. The figure was taken and adapted with permission from Ref. [7] © 2016, Elsevier Ltd.

Muonic capture starts in the outer shells of an atom, around  $n = 14$ , and the first low energy transitions interact with the outer electrons giving a strong Auger effect. As  $n$  decreases, generally from  $n = 5$ , radiative transitions become dominant, with the emission of high energy X-rays. As the muon arrives at the  $1s$  level, it can either decay or be captured by the nuclei of the atom. If the atomic nuclei is heavier than magnesium, capture by the nuclei is more likely to occur: the nucleus goes to an excited state that can lead to the emission of one or more neutrons and gamma rays. For a complete survey of muon capture and general applications, we recommend [9–11].

Given the bigger mass of the muon compared to that of the electron, muonic X-rays are highly energetic (from 0.01 MeV to 6 MeV), even for low Z materials (Figure 2). In most cases, the probability of the muon’s atomic capture is estimated to be proportional to the total number of electrons, as reported in Fermi and Teller [12] (although, some detailed models have been developed to account for some inconsistencies [13–15]). The detection of these high energy X-rays (and gamma) emitted from the muonic atom is the basis of the technique. Since the radiations are characteristic of the emitting atom (Figure 3), muonic atom X-ray spectroscopy is a very effective probe for non-destructive elemental characterization.

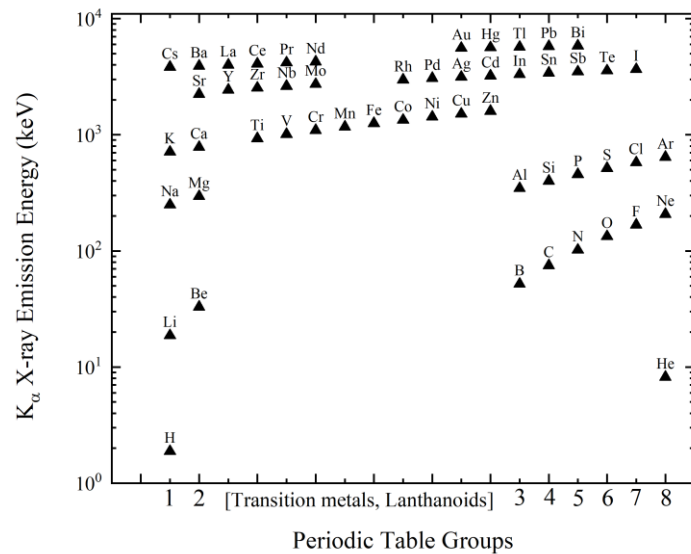


**Figure 2.** K-alpha energy values for the elements of the periodic table. Values are listed in [8,12]. Data was taken and adapted with permission from Ref. [7] © 2016, Elsevier Ltd.

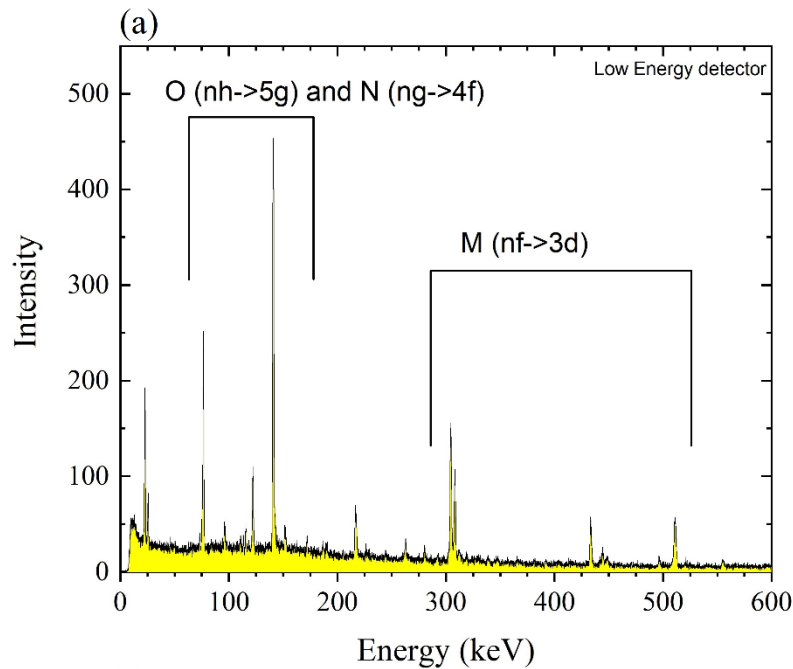


**Figure 3.** Cont.

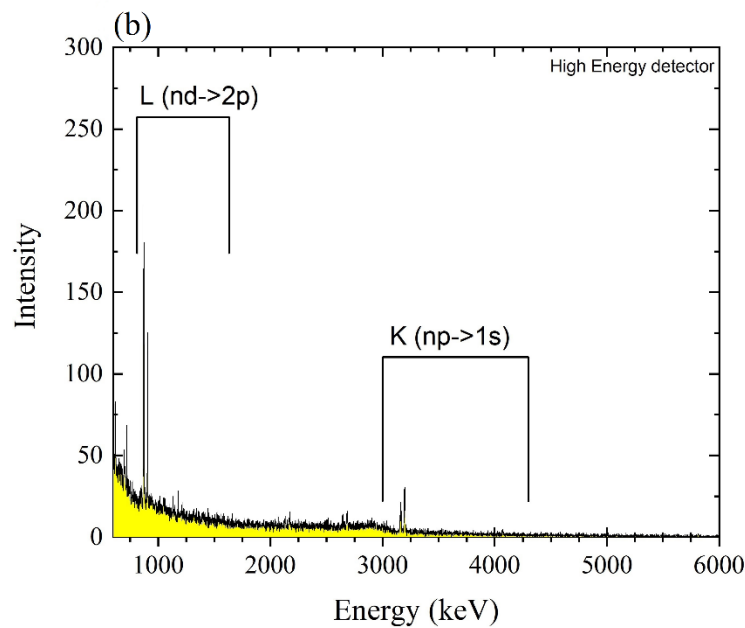


**Figure 3.** A typical pure silver spectrum. (a) With low energy detectors (up to 1 MeV), low energy transitions are detected. Since the muon travels to the nucleus across the energy states of the muonic atom, most of the transition can be detected; (b) high energy transition of silver. Data was taken and adapted from [16].

## 2.2. Muon Production and Muon Beamlines

In nature, muons are produced by the interaction of cosmic rays with the particles present in the atmosphere: there is about 1 muon/second striking on your palm as you read this article. However, to conduct negative muon experiments for elemental analysis requires a greater data rate. These increased data rates are achieved by using a proton accelerator in which the protons (with energies greater than 500 MeV) strike a target, often carbon. If any of these protons collide with a proton/neutron from the carbon target, it will result in the production of pions. In this case, the negative pions decay into negative muons, after about ~26 ns. In the muon beamline, initially, the pions are extracted from the carbon target: these decay in-flight into muons and the muons are transported to an area where the instrument and material of interest is placed. An example beamline is shown in Figure 4. The beam of muons is focused by the quadrupole magnets and the momentum (or energy) of the muons is controlled by the bending (or dipole) magnets. By controlling the momentum/energy, the penetration depth of the muons can be controlled. The momentum can be varied from 15 MeV/c to 120 MeV/c at ISIS, these of course will vary slightly from facility to facility. The penetration depth,  $R$ , can be determined by:

$$R = ap^{3.5}$$

where  $a$  is inversely proportional to the stopping power (which only slightly depends on the element) and  $p$  is the momentum.

There are a number of programs that can model the stopping profile, e.g., GEANT4, G4beamline, SRIM/TRIM [17–19]. A popular and easy-to-use program is SRIM/TRIM, which can simulate these stopping profiles, and may give a more accurate result, by including contributions from many physical processes. A typical maximum penetration depth is about 1 cm in a metal (e.g., copper, silver, iron) and more in less dense materials (e.g., carbon ~2.8 cm and water ~6.1 cm). These calculations have been confirmed experimentally by some studies [7,20,21], which also show the depth selectivity (Figure 5).

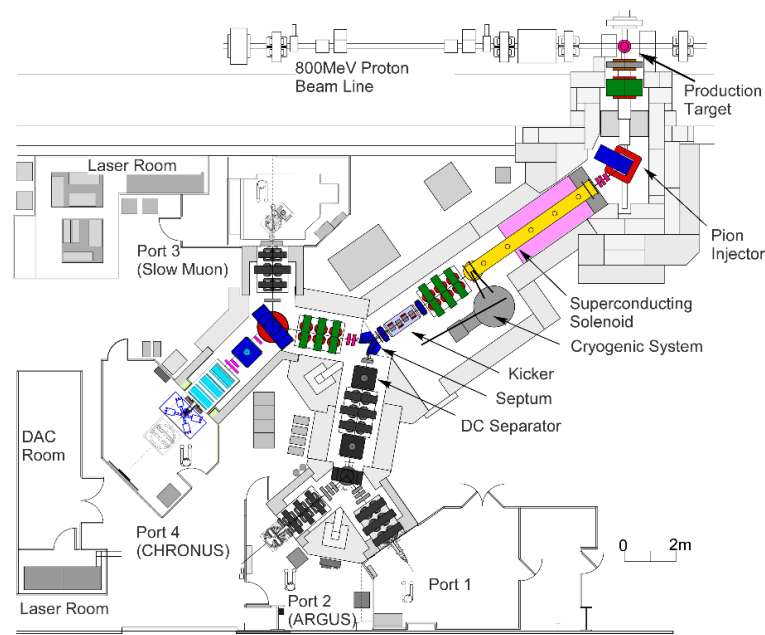


**Figure 4.** A schematic of the RIKEN-RAL beamline based at ISIS. Elemental analysis is currently performed at Port 4. The figure was taken and adapted, with permission from Ref. [7] © 2016 Elsevier Ltd.

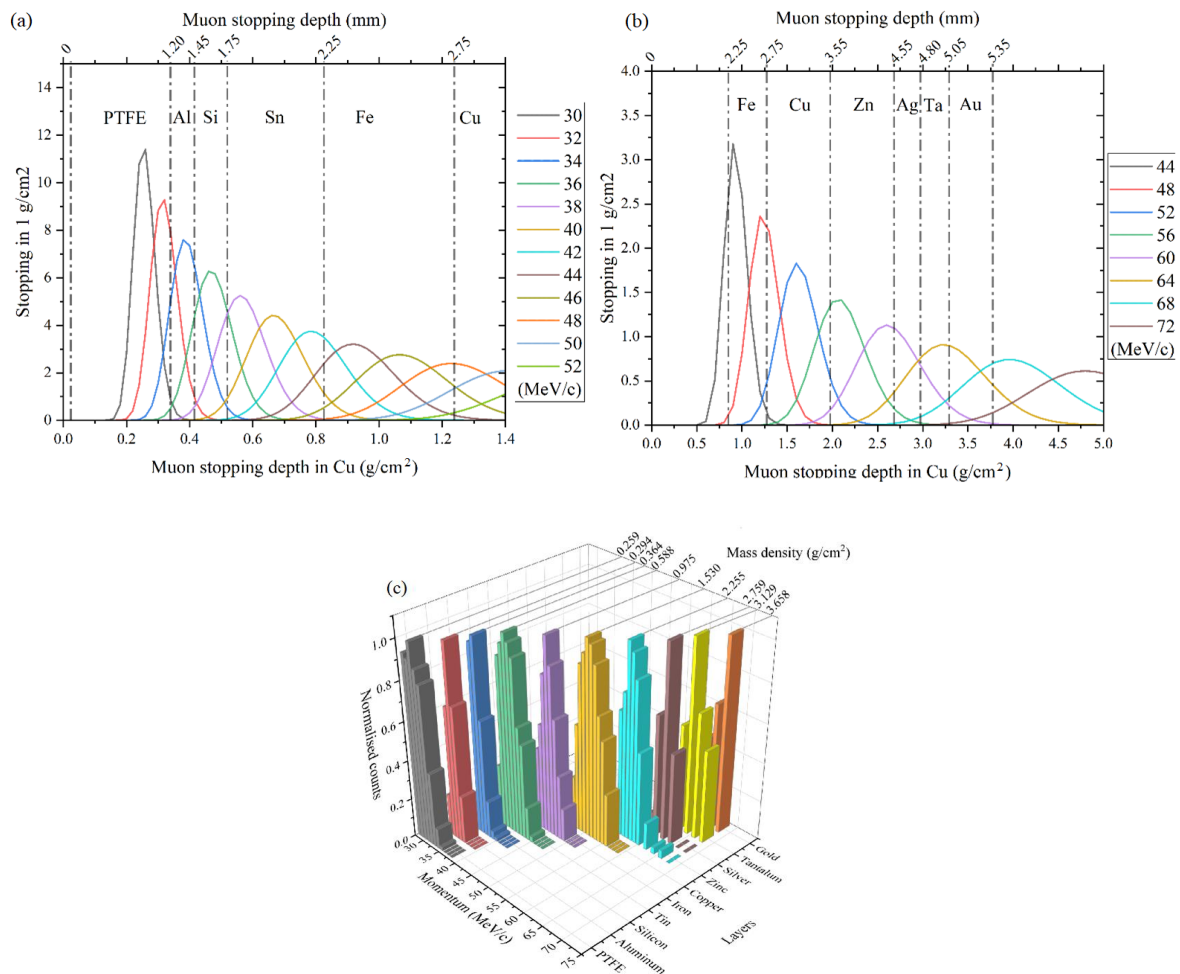


**Figure 5.** Muon depth distribution over a set of different momentum: (a) lower momentum; (b) higher momentum; (c) characteristic X-ray energy distribution. (a,b) The stopping depth was calculated by

taking copper as reference material, taking into account a momentum spread of 4%. The expected locations of the sample material boundary in this reference scale are shown by the dotted vertical lines, while the accumulative thickness is reported on the top axis. For a more detailed survey on particle ranges in material, see Section 34 “Passage of particles through matter” (Figure 34.4) in [22]. (c) The 3D graph shows the distribution of the characteristic muonic X-ray intensity of the elements present in the different layers, with the penetration depth (in  $\text{g}/\text{cm}^2$ ) reported on the top axis. The data and the figure were taken and adapted from Ref. [23].

### 2.3. Muon Instrumentation

Muonic X-ray instruments for cultural heritage experiments are currently installed at J-PARC and MuSIC (Japan) and ISIS (UK) muon facilities [24–26] and under development at PSI (Switzerland) [27] and TRIUMF (Canada). Generally, the instruments consist of several detectors placed around the sample position, as in Figure 6. In most cases, high purity germanium detectors are in place, but Si(Li) detectors can also be used. The latter, however, are limited to low energy measurements (up to 100 keV) and for measuring high-energy muonic X-rays, high-purity germanium detectors are a more convenient choice. Germanium detectors can cover a wide energy range, from a few keV to tens of MeV, as the range depends on the size, quality and geometry of the crystal [28,29]. Figure 6 shows the current setup at ISIS—to improve collection efficiency and optimise data collection, two different types of detectors with different energy ranges are placed upstream and downstream with respect to the sample position (high energy from 100 keV to 8 MeV and low energy from 10 keV to 1 MeV).

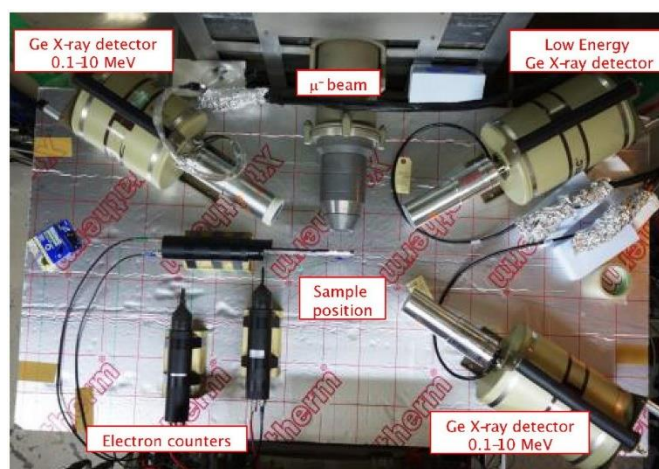


**Figure 6.** The experimental setup at the ISIS muon facility. Thanks to the flexibility of the experimental setup (i.e., the detectors being easily moved), samples of different shapes and sizes can be measured. The figure was taken and adapted with permission from Ref. [7] © 2016, Elsevier Ltd.

### 3. Application to Cultural Heritage Science

In this section, we will review some of the latest work regarding cultural heritage applications. The first application of the negative muons for the characterization of material is dated back to the 1980s [30–32], but only in the last ten years, applications for cultural heritage have been developed, especially for elemental characterization and depth profile studies. An initial study on the characterization of archaeological artefacts was carried on by analyzing a Chinese bronze mirror and a bronze horse model in Japan [20]. As for elemental characterization, depth profiling was also carried out at ISIS, where a multilayered sample was studied by varying the beam energy, thus obtaining information about all the layers [7,23] (Figure 5).



### 3.1. Coinage Debasement

Among all archaeological findings, coins are one of the best tools for historians to assess the fiscal health of the issuing state. Lots of studies have been carried out, but most of them, when non-destructive, could only probe the surface of the sample, or destructive techniques are used. Muonic X-ray spectroscopy, instead, can penetrate deep into materials and can give information about the bulk of the coin, especially when debasement is expected. Debasement is a reduction in the quality of the coin, where the surface is enriched in precious material, such as gold or silver, while the bulk contains less precious materials such as copper [33]. For example, towards the end of the Roman empire, silver coins witnessed a strong debasement: most of them were enriched on the surface to make the coin appear as pure silver, covering the debasement of the alloy. This was conducted by treating the coin with an organic acid that left a silver enriched surface by stripping the copper out of the alloy. In Hampshire et al. [34], a Julia Domna coin was analysed by scanning the material with a different momentum, from 17 MeV/c to 35 MeV/c.

Alongside the depth profiling, elemental analysis was performed. From the momentum scan, it is visible that at low momentum (surface or near-surface) only silver peaks are visible while going further into the sample, copper peaks are present (Figure 7a). The depth dependency is confirmed also by the elemental analysis, which clearly shows a surface enrichment of about 100  $\mu\text{m}$  thickness (Figure 7b).

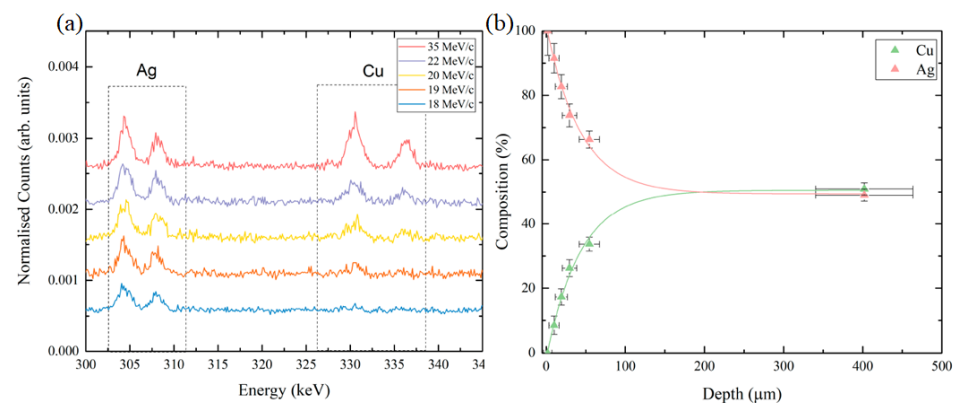


**Figure 7.** (a) Momentum scan of the sample. At low momentum, copper is absent; (b) composition of the alloy. The data obtained from the analysis are in agreement with the literature [35]. The data was taken and adapted from Ref. [34].

Coin debasement was not only mastered by the Romans: in Ninomiya et al. [21], a Japanese Tempo-koban gold coin (19th Century) was analysed with a momentum scan from  $\sim 6$  MeV/c to  $\sim 15$  MeV/c. The coin was already known to have a gold enrichment on the surface from other analyses, but with a strong composition bias. With this muon scan, it was possible to determine a change in gold content from the surface to the core (Figure 8). This was determined by comparing the intensity ratio of Au/Ag. The results of the analysis clearly show a higher amount of gold around the surface of the coin. Gold then, decreases in the core, aligning to other measurement values (around 57%). As in the previous example, the results are consistent with those of the literature, using other analysis methods.

Another study on Japanese coins was carried out on two Tempo-Tsuho coins [36]. In this case, muon spectroscopy was used to reveal the differences between the real coin and the counterfeit, which from eye inspection were very similar. The result of the analysis clearly shows a different composition of the two coins, as reported in Table 1. Here, the results are compared with XRF: the difference in the values could be due to the different spatial regions investigated with XRF, or from the contribution of oxide layers. Muon data can be more representative in this case: the two bronze coins seem to have the same appearance, but they have significantly different elemental compositions.

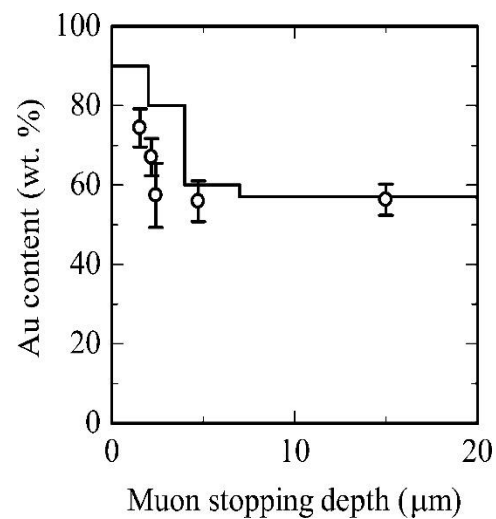


**Figure 8.** Gold variation within the sample thickness. Reprinted with permission from “Nondestructive Elemental Depth-Profiling Analysis by Muonic X-ray Measurement”. K. Ninomiya, M. K. Kubo, T. Nagatomo, W. Higemoto, T. U. Ito, N. Kawamura, P. Strasser, K. Shimomura, Y. Miyake, T. Suzuki, Y. Kobayashi, S. Sakamoto, A. Shinohara, T. Sait. 2015, *Analytical Chemistry*, Vol. 87, pp. 4597–4600, Ref. [21] Copyright (2015) American Chemical Society.

**Table 1.** Elemental composition of the two coins in wt.%. The real coin is the Tempo-Tsuho (Edo), while the counterfeit is the Tempo-Tsuho (Mito). Results are compared with XRF. Data was taken and adapted from [36].

Sample	Element	Muonic X-ray Measurement [wt.%]	X-ray Fluorescence [wt.%]
Tempo-Tsuho (Edo)	Cu	$77.7 \pm 1.6$	$77.77 \pm 0.01$
	Sn	$12.5 \pm 1.5$	$14.45 \pm 0.54$
	Pb	$9.8 \pm 1.5$	$7.79 \pm 0.16$
Tempo-Tshuo (Mito)	Cu	$69.0 \pm 1.9$	$73.64 \pm 0.01$
	Sn	$9.9 \pm 1.3$	$12.18 \pm 0.41$
	Pb	$21.1 \pm 2.6$	$14.17 \pm 0.12$

In periods of better stability instead, debasement wasn't required. In Green et al. [37], a study on three Roman gold coins is presented. The paper compares the results from XRF analysis with the one from muonic X-ray emission. From XRF, the three coins show a high concentration of gold, almost full purity for two out of three. The issue of XRF, however, is that it only probes the first few microns of a material, so it is not representative of the alloy. Therefore, a measurement with muons is carried out. In this case, only two momenta were selected: 40 MeV/c for investigating the core of the coin and 18 MeV/c for the near-surface (Figure 9a,b). The results from the muon analysis are in remarkable agreement with that of XRF and no surface enrichment was found on these coins (Table 2). Results show that Roman gold coins were not surface-enriched, different to the silver coins. With this work, muon analysis provided a new set of information for the study of Roman coinage, showing that for gold coins, the surface is representative of the bulk.

### 3.2. Elemental Analysis of Bronze Artefacts

Copper and bronze were used extensively through time, leaving us with a wealth of cultural objects that are just waiting to be studied. Over the last years, some bronze artefacts were analysed by means of muon spectroscopy. In Ninomiya et al. [36], a Chinese bronze mirror (Seiun-Kyo) was measured. The mirror was measured with a momentum of 22 MeV/c. From the data analysis, results showed it composed of a ternary alloy (copper,



tin and lead) with smaller amounts of other elements. To perform elemental composition, three specific peaks were chosen: 115 keV for copper, 159 keV for tin and 233 keV for lead. The elemental composition of the mirror was found to be 71.8% copper, 22.1% tin and 6.1% of lead.

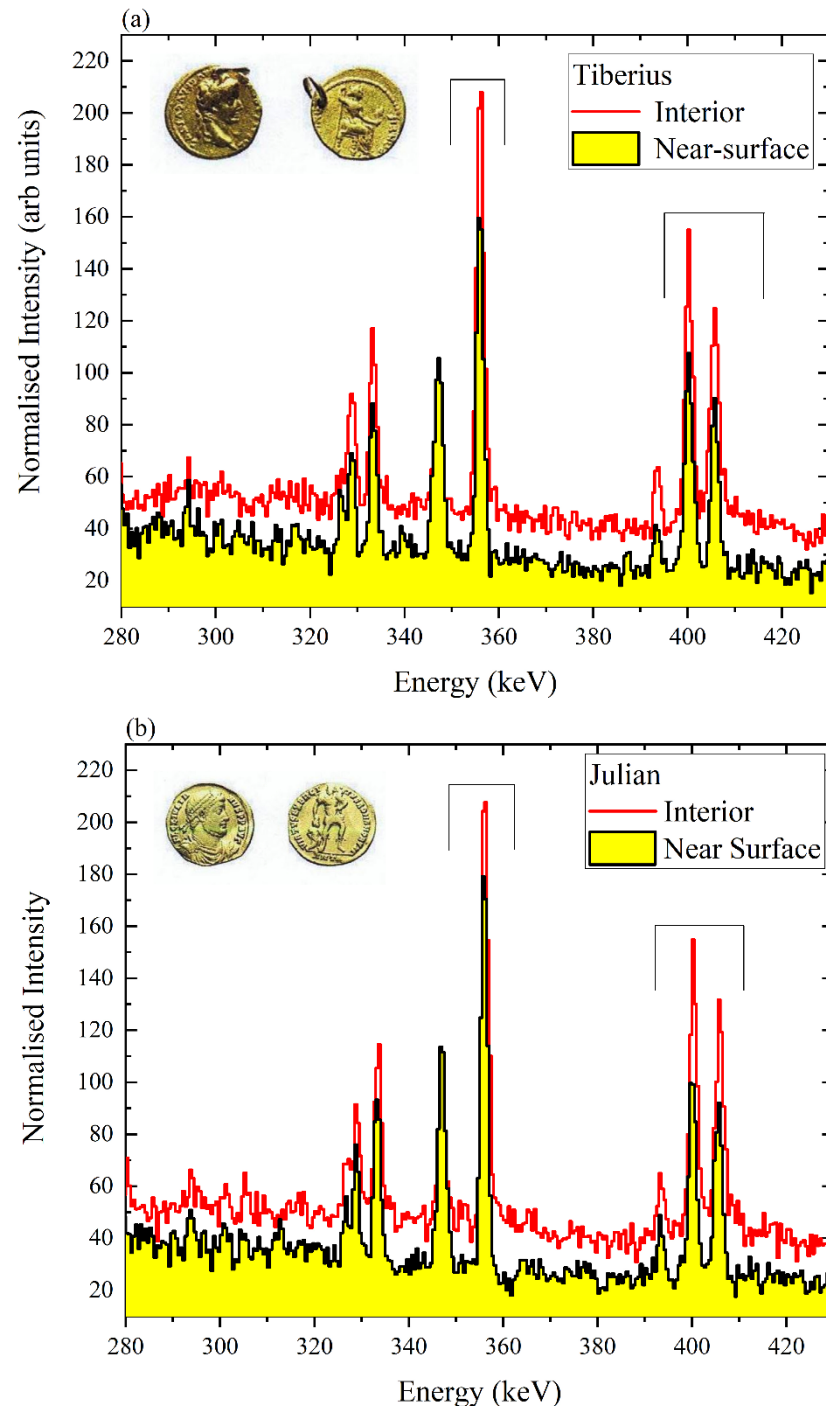


**Figure 9.** Spectra of Tiberius (a) and Julian (b) measured coins. Gold is present in both coins with a double peak at 400 keV and 406 keV and a gamma peak at 355 keV. As mentioned before, the surface (yellow) is representative of the interior (red). Reprinted with permission from Ref [37] © 2021, Elsevier Ltd.

**Table 2.** Comparison of the XRF and Muon analysis. The results of the muon analysis are reported in the right columns. It is evident that the information coming from the surface (at 18 MeV/c) and the core (40 MeV/c) have no relevant difference: in this case, the surface is representative of the bulk composition. The data was taken from and adapted with permission from Ref. [37] © 2021, Elsevier Ltd.

Coin	XRF			$\mu$ XES—40 MeV/c			$\mu$ XES—18 MeV/c		
	Mean Au [wt.%]	Mean Ag [wt.%]	Mean Cu [wt.%]	Au [wt.%]	Ag [wt.%]	Cu [wt.%]	Au [wt.%]	Ag [wt.%]	Cu [wt.%]
<b>Tiberius</b> [AD 14–37]	99.73 (0.1)%	0.27 (0.01)%	-	>99%	<1%	-	>99%	<1%	-
<b>Hadrian</b> [AD 134–138]	99.55 (0.1)%	0.45 (0.01)%	-	>99%	<1%	-	>99%	<1%	-
<b>Julian II</b> [AD 361–363]	95.58 (0.3)%	4.18 (0.03)%	0.24 (0.02)%	96 (1)%	4 (1)%	-	96 (1)%	4 (1)%	-

Similarly, in Clemenza et al. [23] and Marcucci et al. ([38], forthcoming), Nuragic “votive” ships were characterized. Particularly, in Marcucci, two votive ships coming from the tomb of the “Tre Navicelle” were irradiated at Port 4 of the RIKEN-RAL facility. Votive ships are a unique production of the Sardinian metallurgy and in this work, the elemental composition was investigated.

From the data analysis, results show the hull of the two samples to be composed of a ternary alloy (copper, tin, lead), with a lower concentration of tin in the head and the mast, balanced by a higher concentration of lead. For sample n.6779 (Figure 10a, points A, D, E) the average composition is: copper  $76.4 \pm 0.3$  wt.%, tin  $12.2 \pm 0.2$  wt.% and lead  $11.5 \pm 0.3$  wt.%. While for sample n.6780 (Figure 10b, points A, D, E), the average composition is: copper  $77.4 \pm 0.5$  wt.%, tin  $10.7 \pm 0.3$  wt.%, and lead  $11.8 \pm 0.5$  wt.%. The variation between the composition of the head and the mast, compared to the hull, is used to make assumptions about the manufacturing technique. Here, the authors suggest that the boats were made by a two-step casting process: the first part involved the hull, while the head and the mast were added in a second phase. These two pieces were intentionally made with a different alloy, rich in lead, as reported in Figure 11; a high amount of lead, indeed, helps with the casting of complex details, since the fluidity of the alloy is increased.

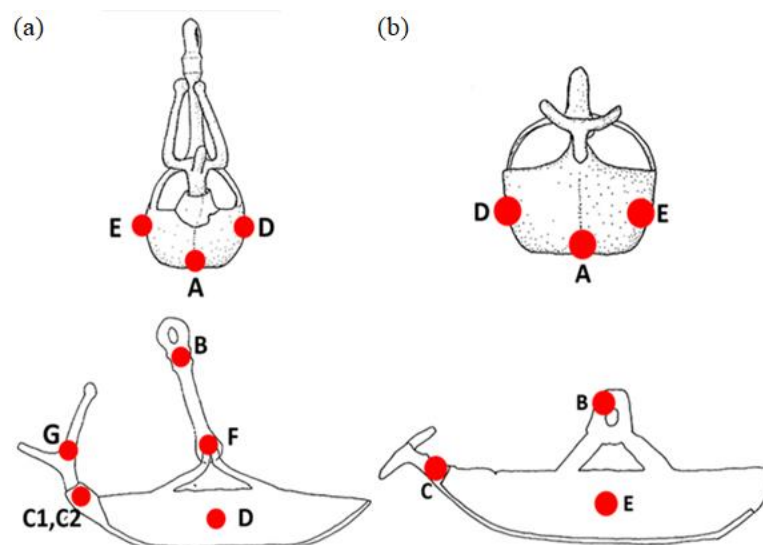


**Figure 10.** Drawing of the two samples and measured areas (red). (a) Model n.6779; (b) model n.6780.

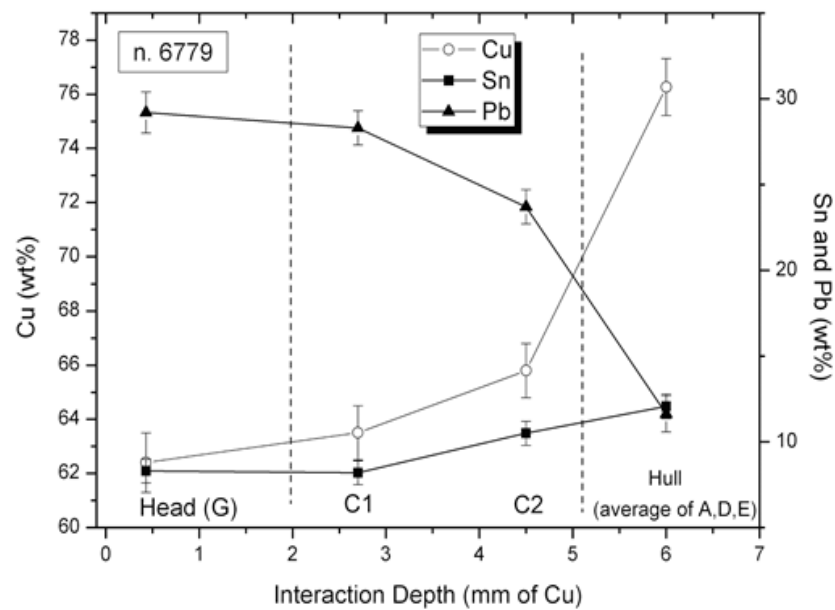


**Figure 11.** Depth profile of copper, tin and lead concentration (wt.%) of the neck of the boat in boat n.6779. The tin concentration is similar in all the measured areas, while lead and copper vary more significantly.

### 3.3. Meteorites

Muonic X-ray spectroscopy can be a very useful tool for the study of extraterrestrial samples, especially for the analysis of light elements with a non-destructive approach. In Terada et al. [39], a study was carried out on meteorite fragments from carbonaceous chondrites, called Murchinson and Allende. From the results, the former contains more extraterrestrial organic material than the latter, as shown in Table 3.

**Table 3.** The muonic X-rays detected (along with the transitions) in the Murchinson and Allende meteorites and the concentrations of each element. The data was taken and adapted from Ref. [39].

Element and (Transition)	Energy (keV)	Murchison (Counts)	Allende (Counts)
Calcium Ca-(M $\alpha$ )	55	n.d.	53 $\pm$ 23
Magnesium Mg-(L $\alpha$ )	56	896 $\pm$ 66	183 $\pm$ 23
Aluminum Al-(L $\alpha$ )	66	10,796 $\pm$ 130	136 $\pm$ 30
Carbon C-(K $\alpha$ )	75	626 $\pm$ 52	6 $\pm$ 27
Silicon Si-(L $\alpha$ )	76	824 $\pm$ 58	175 $\pm$ 32
Iron Fe-(M $\alpha$ )	94	1319 $\pm$ 63	265 $\pm$ 39
Oxygen O-(K $\alpha$ )	133	4785 $\pm$ 111	800 $\pm$ 38
Potassium K-(L $\alpha$ )	140	n.d.	94 $\pm$ 27
Calcium Ca-(L $\alpha$ )	156	213 $\pm$ 41	83 $\pm$ 28
Aluminum Al-(K $\alpha$ )	346	9542 $\pm$ 100	359 $\pm$ 27
Silicon S-(K $\alpha$ )	516	121 $\pm$ 33	11 $\pm$ 9

The Murchinson meteorite is characterized by a significant signal from carbon, showing that it contains a large amount of organic material, as well as magnesium, carbon, silicon, iron, calcium, and sulphur. On the other hand, only magnesium, silicon, iron, potassium, and calcium were found in the Allende meteorite. In addition to these elements, aluminium has also been observed, but this is reportedly from the sample holder. Besides the multi-component analysis, the study shows another interesting application;

given the possibility of depth profiling, one can measure extraterrestrial samples within their containing tubes, thus avoiding contamination from terrestrial materials. Another study on meteorite fragments is reported in [40]. Muon analysis can be a valid option in this particular field of research, to add further information but also to avoid some of the disadvantages related to other techniques, such as severe radioactivation of the sample, difficulty of bulk analysis and limited sensitivity.

#### 3.4. Organic Materials

Thanks to the ability of the technique to detect low  $Z$  atoms, the analysis of organic materials is feasible. In some early papers [30,41], analysis of biological tissues was performed and in a more recent work, human vertebral bones were investigated [42]. An example of the technique potential is reported in Shimada-Takaura [43]. In this work, the authors analysed some precious glass bottles belonging to the OGATA Koan medicine chests. OGATA Koan (1810–1863) was a physician in the late Edo period and the bottle contained formulated medicines; however, due to the preciousness of the material and the impossibility of opening some of the containers, a non-destructive approach was mandatory. Therefore, muonic X-ray analysis was performed on two bottles, with two different momenta: 40 MeV/c and 55 MeV/c. The two selected momenta were stopped in differing parts of the sample; at 40 MeV/c, information comes from the container (glass), while at 55 MeV/c, information comes from the material in the container. The results show that the medicine is mainly composed of mercury, chlorine, sodium and oxygen, in agreement with the documents that regulated the properties of drugs (mercury and chlorine are assigned to  $\text{HgCl}_2$ , while sodium and oxygen to  $\text{NaCl}$  and  $\text{H}_2\text{O}$ , probably added as additives). This unique approach to the study of a sample is a further example of the quality and potential of the technique.

#### 3.5. Isotopic Analysis

The determination of isotope composition can be a very useful tool for the study of a sample, especially for provenance studies. Most of the research [44,45], however, has a destructive approach; a non-invasive approach could be performed by muon spectroscopy. It has been observed that, especially for heavier elements, there is an isotopic shift in muonic K-line energies. The nuclear size difference of the isotopes (owing to the Coulomb attraction being diluted when the isotope size is bigger) affects the muonic X-ray, resulting in a small shift in these energies. In Ninomiya et al. [46], measurements were performed on lead. Lead is the most common material used for provenance studies since ores can be distinguished by the comparison of lead isotope ratios. In the work, small but measurable shifts were observed in the  $K\alpha$  peaks. Another way of assessing the isotope composition is to use the gamma rays that can be emitted after negative muon capture by the nucleus. As reported in Section 2, if the muon is captured by the nuclei, it could lead to gamma-ray emissions. Hence, the emitted gamma rays can be detected and used to identify the parent nuclide responsible for the emission. There are a number of studies investigating this aspect [47–50] and values are tabulated on the IEAE website [51], while the first experiment with lead is reported in [52].

#### 3.6. Muon Imaging

A new potential improvement to the technique is represented by muon imaging. By placing a detector behind the sample, information about the spatial distribution of the sample can be obtained, especially for light elements. In Hillier et al. [53] and Yabu et al. [54], feasibility studies of muon imaging are reported. In both works, a highly pixelated CdTe detector is used to collect the signal (cadmium telluride is a rather good material for detection, especially in the range of hard X-rays). In [53], a proximity image (Figure 12) was obtained by placing the detector behind the sample holder and measuring it at 40 MeV/c.

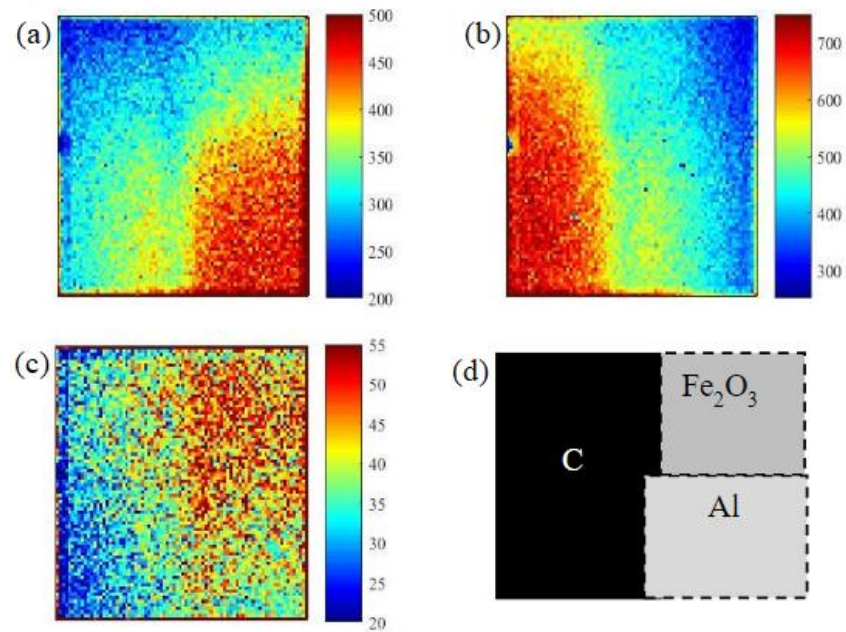


**Figure 12.** The number of events at (a) 66 keV (Aluminum), (b) 75 keV (Carbon) and (c) 131 keV (Oxygen), corresponding to the position of the material in the sample (d). Originally published in JPS Conf. Proc. 21, 011042 (2018). Reprinted with permission from Ref. [53] © 2018 The Author(s) of Ref. [53].

In [54], instead, a pinhole setup was used. In this study, the sample was composed of four different layers, one of which was made of small squares of lithium fluoride, as shown in Figure 13a. From the result, the LiF squares are resolved by the detector, as shown in Figure 13b, which covers the range from 27 keV to 35 keV. These two preliminary studies show the possibility of direct imaging: by adding the information coming from depth profiling, one can develop a three-dimensional analysis.

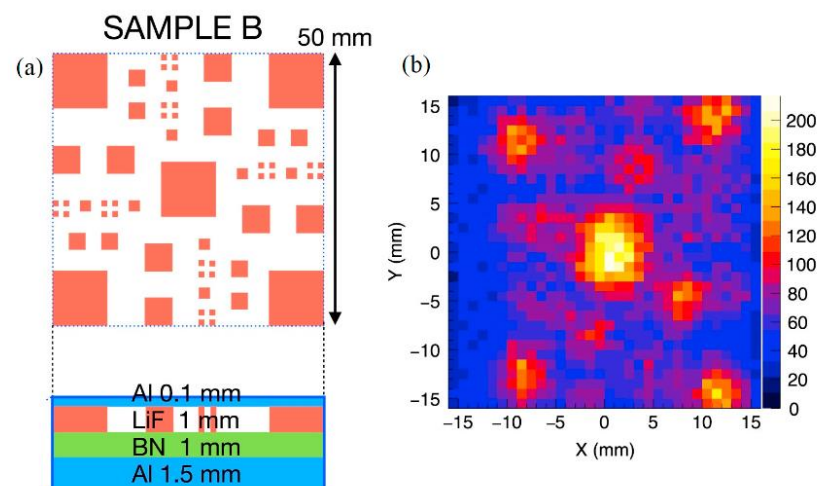


**Figure 13.** (a) Scheme of the sample; (b) position of the fluorine in the sample, within the range from 27 keV to 35 keV. Originally published in JPS Conf. Proc. 21, 011044 (2018). Reprinted with permission from Ref. [54] © 2018 The Author(s) of Ref. [54].

#### 4. Future Developments and Access

Developments are underway at all facilities such that the sensitivity and the accuracy of the technique can be improved. This could be done, for example, by increasing the solid angle coverage of the detectors (i.e., the instrument setup relatively easy) and by

increasing the muon flux (accelerator development, much harder). However, plans are in place to increase data rates by at least one order of magnitude to several orders of magnitude, which will enable a rapid expansion of the technique and/or new instrument plan at muon facilities, such as ISIS and J-PARC. As stated before, the technique utilizes a large accelerator, so the material of interest be to be moved to the facility. There are various routes to obtain access to these facilities, that are dependent on the facility. However, in general for academic research these are free at the point of use and are peer-reviewed; yet, other routes are available, including paying for access.

## 5. Conclusions

Muonic X-ray spectroscopy is still a novel, yet very powerful, technique. The non-destructive approach, the sensitivity to low to high Z atoms and negligible self-absorption of the X-rays make the technique suitable, especially, for cultural heritage research. However, the examples reported in the work show that the fields of applications are many and not strictly correlated to heritage science. They define, though, a technique with enormous potential. Muonic atom X-ray spectroscopy is a multi-elemental technique (from lithium to uranium) able to characterize both the superficial layer and the bulk of the material within the same experiment in a non-destructive way. This is an invaluable characteristic in the field of cultural heritage analysis, especially for ancient coins, since it is capable of detecting surface treatments and enrichments. The technique can also provide information about the manufacturing process of an artefact; due to the energy scan, it is possible to characterize different parts of a sample and see, for example, how pieces were welded together. Furthermore, although it is not yet implemented, the ability to scan the material makes 3D imaging feasible. Finally, future perspectives are represented by the isotopic analysis; owing to gamma prompt reactions and energy shifts in the muonic X-rays (due to the mass differences), it is possible to detect the presence of different isotopes in the material. This will be of inestimable value for provenance studies, especially for lead isotopes, since the techniques used nowadays have a destructive approach. In this way, rare and precious material that cannot be studied because of the prohibition on sampling could be analysed in a non-destructive way.

**Author Contributions:** Conceptualization, A.D.H., M.C. (Matteo Cataldo) and M.C. (Massimiliano Clemenza); writing—original draft preparation, M.C. (Matteo Cataldo); writing—review and editing, A.D.H., M.C. (Matteo Cataldo), M.C. (Massimiliano Clemenza) and K.I. All authors have read and agreed to the published version of the manuscript.

**Funding:** The author (Matteo Cataldo) PhD is co-funded by ISIS and UNIMIB under the studentship agreement No. S2 2021 002 CN8647.

**Institutional Review Board Statement:** Not applicable.

**Informed Consent Statement:** Not applicable.

**Data Availability Statement:** Not applicable.

**Acknowledgments:** The authors acknowledge the ISIS Neutron and Muon Source, STFC/UKRI, the University of Milano Bicocca and the INFN CHnet for funding the research and development of Muon spectroscopy techniques at RIKEN-RAL facility.

**Conflicts of Interest:** The authors declare no conflict of interest.

## References

1. Mantler, M.; Schreiner, M. *X-ray Fluorescence Spectrometry in Art and Archaeology*; John Wiley & Sons: Hoboken, NJ, USA, 2000; Volume 29, pp. 3–17. [\[CrossRef\]](#)
2. Schreiner, M.; Melcher, M.; Uhlir, K. Scanning electron microscopy and energy dispersive analysis: Applications in the field of cultural heritage. *Anal. Bioanal. Chem.* **2006**, *387*, 737–747. [\[CrossRef\]](#) [\[PubMed\]](#)
3. Mahnke, H.-E.; Denker, A.; Salomon, J. Accelerators and x-rays in cultural heritage investigations. *Comptes Rendus. Phys.* **2009**, *10*, 660–675. [\[CrossRef\]](#)



4. Giorgi, G. Overview of Mass Spectrometric Based Techniques Applied in the Cultural Heritage Field. In *Organic Mass Spectrometry in Art and Archaeology*; John Wiley & Sons: Hoboken, NJ, USA, 2009; pp. 37–74. [[CrossRef](#)]
5. Kardjilov, N.; Festa, G. *Neutron Methods for Archaeology and Cultural Heritage*; Springer: Cham, Switzerland, 2017; Available online: <http://link.springer.com/10.1007/978-3-319-33163-8> (accessed on 6 April 2022).
6. Alfeld, M.; Broekaert, J.A.C. Mobile depth profiling and sub-surface imaging techniques for historical paintings—A review. *Spectrochim. Acta Part B Atomic Spectrosc.* **2013**, *88*, 211–230. [[CrossRef](#)]
7. Hillier, A.; Paul, D.; Ishida, K. Probing beneath the surface without a scratch—Bulk non-destructive elemental analysis using negative muons. *Microchem. J.* **2015**, *125*, 203–207. [[CrossRef](#)]
8. Engfer, R.; Schneuwly, H.; Vuilleumier, J.L.; Walter, H.K.; Zehnder, A. Charge-distribution parameters, isotope shifts, isomer shifts, and magnetic hyperfine constant from muonic atoms. *Atomic Data Nucl. Data Tables* **1974**, *14*, 509–597. [[CrossRef](#)]
9. Measday, D. The nuclear physics of muon capture. *Phys. Rep.* **2001**, *354*, 243–409. [[CrossRef](#)]
10. Blundell, S.J.; de Rienzi, R.; Lancaster, T.; Pratt, F.L. *Muon Spectroscopy: An Introduction*; Oxford University Press: Oxford, UK, 2021.
11. Hillier, A.D.; Hampshire, B.; Ishida, K. Depth-Dependent Bulk Elemental Analysis Using Negative Muons. In *Handbook of Cultural Heritage Analysis*; D’Amico, S., Venuti, V., Eds.; Springer: Cham, Switzerland, 2022; pp. 23–43. [[CrossRef](#)]
12. Fermi, E.; Teller, E. The Capture of Negative Mesotrons in Matter. *Phys. Rev.* **1947**, *72*, 399–408. [[CrossRef](#)]
13. Daniel, H. Coulomb capture of muons and atomic radius. *Z. Physik. A Atomic Nucl.* **1979**, *291*, 29–31. [[CrossRef](#)]
14. Von Egidy, T.; Jakubassa-Amundsen, D.H.; Hartmann, F.J. Calculation of muonic Coulomb-capture probabilities from electron binding energies. *Phys. Rev. A* **1984**, *29*, 455–461. [[CrossRef](#)]
15. Schneuwly, H.; Pokrovsky, V.; Ponomarev, L. On coulomb capture ratios of negative mesons in chemical compounds. *Nucl. Phys. A* **1978**, *312*, 419–426. Available online: [http://inis.iaea.org/search/search.aspx?orig\\_q=RN:10456796](http://inis.iaea.org/search/search.aspx?orig_q=RN:10456796) (accessed on 16 February 2022). [[CrossRef](#)]
16. Hillier, A.D.; Butcher, K.; Hampshire, B. Isotope analysis of materials using muonic X-ray and gammas. In *ISIS Neutron and Muon Source*; Science and Technology Facilities Council: Swindon, UK, 2019.
17. Agostinelli, S.; Allison, J.; Amako, K.; Apostolakis, J.; Araujo, H.; Arce, P.; Asai, M.; Axen, D.; Banerjee, S.; Barrand, G.; et al. Geant4—A simulation toolkit. *Nucl. Instrum. Methods Phys. Res. Sect. A Accel. Spectrom. Detect. Assoc. Equip.* **2003**, *506*, 250–303. [[CrossRef](#)]
18. Hurtado, S.; León, M.G.; García-Tenorio, R. GEANT4 code for simulation of a germanium gamma-ray detector and its application to efficiency calibration. *Nucl. Instrum. Methods Phys. Res. Sect. A Accel. Spectrom. Detect. Assoc. Equip.* **2004**, *518*, 764–774. [[CrossRef](#)]
19. Ziegler, J.F.; Ziegler, M.D.; Biersack, J.P. SRIM—The stopping and range of ions in matter. *Nucl. Instrum. Methods B* **2010**, *268*, 1818–1823. [[CrossRef](#)]
20. Kubo, M.K.; Moriyama, H.; Tsuruoka, Y.; Sakamoto, S.; Koseto, E.; Saito, T.; Nishiyama, K. Non-destructive elemental depth-profiling with muonic X-rays. *J. Radioanal. Nucl. Chem. Artic.* **2008**, *278*, 777–781. [[CrossRef](#)]
21. Ninomiya, K.; Kubo, M.K.; Nagatomo, T.; Higemoto, W.; Ito, T.U.; Kawamura, N.; Strasser, P.; Shimomura, K.; Miyake, Y.; Suzuki, T.; et al. Nondestructive Elemental Depth-Profiling Analysis by Muonic X-ray Measurement. *Anal. Chem.* **2015**, *87*, 4597–4600. [[CrossRef](#)]
22. Particle Data Group; Zyla, P.A.; Barnett, R.M.; Beringer, J.; Dahl, O.; Dwyer, D.A.; Groom, D.E.; Lin, C.-J.; Lugovsky, K.S.; Pianori, E.; et al. Review of Particle Physics. *Prog. Theor. Exp. Phys.* **2020**, *2020*, 083C01. [[CrossRef](#)]
23. Clemenza, M.; Bonesini, M.; Carpinelli, M.; Cremonesi, O.; Fiorini, E.; Gorini, G.; Hillier, A.; Ishida, K.; Menegolli, A.; Mocchiutti, E.; et al. Muonic atom X-ray spectroscopy for non-destructive analysis of archeological samples. *J. Radioanal. Nucl. Chem. Artic.* **2019**, *322*, 1357–1363. [[CrossRef](#)]
24. Ninomiya, K.; Nagatomo, T.; Kubo, M.K.; Strasser, P.; Kawamura, N.; Shimomura, K.; Miyake, Y.; Saito, T.; Higemoto, W. Development of elemental analysis by muonic X-ray measurement in J-PARC. *J. Phys. Conf. Ser.* **2010**, *225*, 012040. [[CrossRef](#)]
25. Hillier, A.D.; Lord, J.S.; Ishida, K.; Rogers, C. Muons at ISIS. *Philos. Trans. R. Soc. London. Ser. A Math. Phys. Eng. Sci.* **2018**, *377*, 20180064. [[CrossRef](#)]
26. Hino, Y.; Kuno, Y.; Sato, A.; Sakamoto, H.; Matsumoto, Y.; Tran, N.; Hashim, I.; Fukuda, M.; Hayashida, Y.; Ogitsu, T.; et al. A Highly intense DC muon source, MuSIC and muon CLFV search. *Nucl. Phys. B Proc. Suppl.* **2014**, *253–255*, 206–207. [[CrossRef](#)]
27. Biswas, S.; Gerchow, L.; Luetkens, H.; Prokscha, T.; Antognini, A.; Berger, N.; Cocolios, T.E.; Dressler, R.; Indelicato, P.; Jungmann, K.; et al. Characterization of a Continuous Muon Source for the Non-Destructive and Depth-Selective Elemental Composition Analysis by Muon Induced X- and Gamma-rays. *Appl. Sci.* **2022**, *12*, 2541. [[CrossRef](#)]
28. Jenkins, D. *Radiation Detection for Nuclear Physics*; IOP Publishing: Bristol, UK, 2020. [[CrossRef](#)]
29. Giuntini, L.; Castelli, L.; Massi, M.; Fedi, M.; Czelusniak, C.; Gelli, N.; Liccioli, L.; Giambi, F.; Ruberto, C.; Mazzinghi, A.; et al. Detectors and Cultural Heritage: The INFN-CHNet Experience. *Appl. Sci.* **2021**, *11*, 3462. [[CrossRef](#)]
30. Reidy, J.J.; Hutson, R.L.; Daniel, H.; Springer, K. Use of muonic x-rays for nondestructive analysis of bulk samples for low Z constituents. *Anal. Chem.* **1978**, *50*, 40–44. [[CrossRef](#)]
31. Köhler, E.; Bergmann, R.; Daniel, H.; Ehrhart, P.; Hartmann, F. Application of muonic X-ray techniques to the elemental analysis of archeological objects. *Nucl. Instrum. Methods Phys. Res.* **1981**, *187*, 563–568. [[CrossRef](#)]
32. Daniel, H. Application of X-rays from negative muons. *Nucl. Instrum. Methods Phys. Res.* **1984**, *3*, 65–70. [[CrossRef](#)]

33. Moreno-Suárez, A.; Ager, F.; Scrivano, S.; Ortega-Feliu, I.; Gómez-Tubío, B.; Respaldiza, M. First attempt to obtain the bulk composition of ancient silver–copper coins by using XRF and GRT. *Nucl. Instrum. Methods Phys. Res. Sect. B Beam Interact. Mater. Atomic* **2015**, *358*, 93–97. [[CrossRef](#)]
34. Hampshire, B.V.; Butcher, K.; Ishida, K.; Green, G.; Paul, D.M.; Hillier, A.D. Using Negative Muons as a Probe for Depth Profiling Silver Roman Coinage. *Heritage* **2019**, *2*, 400–407. [[CrossRef](#)]
35. Ortega-Feliu, I.; Moreno-Suárez, A.; Gómez-Tubío, B.; Ager, F.; Respaldiza, M.; García-Dils, S.; Rodríguez-Gutiérrez, O. A comparative study of PIXE and XRF corrected by Gamma-Ray Transmission for the non-destructive characterization of a gilded roman railing. *Nucl. Instrum. Methods Phys. Res. Sect. B Beam Interact. Mater. Atomic* **2010**, *268*, 1920–1923. [[CrossRef](#)]
36. Ninomiya, K.; Kubo, M.K.; Strasser, P.; Nagatomo, T.; Kobayashi, Y.; Ishida, K.; Higemoto, W.; Kawamura, N.; Shimomura, K.; Miyake, Y.; et al. Elemental Analysis of Bronze Artifacts by Muonic X-ray Spectroscopy. *JPS Conf. Proc.* **2015**, *8*, 033005. [[CrossRef](#)]
37. Green, G.A.; Ishida, K.; Hampshire, B.V.; Butcher, K.; Pollard, A.; Hillier, A.D. Understanding Roman Gold Coinage Inside Out. *J. Archaeol. Sci.* **2021**, *134*, 105470. [[CrossRef](#)]
38. Marcucci, G.; Oliva, P.; Bonesini, M.; Carpinelli, M.; Cremonesi, O.; Depalmas, A.; Di Martino, D.; Fiorini, E.; Gorini, G.; Hillier, A.D.; et al. Muonic Atom X-rays Spectroscopy for elemental characterization of bronze nuragic lamps found in the ‘Tre Navicelle’ Tomb’. *J. Archaeom.* *submitted*.
39. Terada, K.; Ninomiya, K.; Osawa, T.; Tachibana, S.; Miyake, Y.; Kubo, M.K.; Kawamura, N.; Higemoto, W.; Tsuchiyama, A.; Ebihara, M.; et al. A new X-ray fluorescence spectroscopy for extraterrestrial materials using a muon beam. *Sci. Rep.* **2014**, *4*, 5072. [[CrossRef](#)] [[PubMed](#)]
40. Terada, K.; Sato, A.; Ninomiya, K.; Kawashima, Y.; Shimomura, K.; Yoshida, G.; Kawai, Y.; Osawa, T.; Tachibana, S. Non-destructive elemental analysis of a carbonaceous chondrite with direct current Muon beam at MuSIC. *Sci. Rep.* **2017**, *7*, 15478. [[CrossRef](#)] [[PubMed](#)]
41. Hutson, R.L.; Reidy, J.J.; Springer, K.; Daniel, H.; Knowles, H.B. Tissue Chemical Analysis with Muonic X rays. *Radiology* **1976**, *120*, 193–198. [[CrossRef](#)]
42. Hosoi, Y.; Watanabe, Y.; Sugita, R.; Tanaka, Y.; Nagamine, K.; Ono, T.; Sakamoto, K. Non-destructive elemental analysis of vertebral body trabecular bone using muonic X-rays. *Br. J. Radiol.* **1995**, *68*, 1325–1331. [[CrossRef](#)]
43. Shimada-Takaura, K.; Ninomiya, K.; Sato, A.; Ueda, N.; Tampo, M.; Takeshita, S.; Umegaki, I.; Miyake, Y.; Takahashi, K. A novel challenge of nondestructive analysis on OGATA Koan’s sealed medicine by muonic X-ray analysis. *J. Nat. Med.* **2021**, *75*, 532–539. [[CrossRef](#)]
44. Cuchí-Oterino, J.A.; Penanes, P.A.; Martín-Gil, J.; Moldovan, M.; Aragón, I.A.; Martín-Ramos, P. Mineral provenance of Roman lead objects from the Cinca River basin (Huesca, Spain). *J. Archaeol. Sci. Rep.* **2021**, *37*, 102979. [[CrossRef](#)]
45. Baker, J.; Stos, S.; Waight, T. Lead isotope analysis of archaeological metals by multiple-collector inductively coupled PLASMA mass spectrometry. *Archaeometry* **2006**, *48*, 45–56. [[CrossRef](#)]
46. Ninomiya, K.; Kudo, T.; Strasser, P.; Terada, K.; Kawai, Y.; Tampo, M.; Miyake, Y.; Shinohara, A.; Kubo, K.M. Development of non-destructive isotopic analysis methods using muon beams and their application to the analysis of lead. *J. Radioanal. Nucl. Chem. Artic.* **2019**, *320*, 801–805. [[CrossRef](#)]
47. Backenstoss, G.; Charalambus, S.; Daniel, H.; Hamilton, W.; Lynen, U.; Von Der Malsburg, C.; Poelz, G.; Povel, H. Nuclear  $\gamma$ -rays following muon capture. *Nucl. Phys. A* **1971**, *162*, 541–551. [[CrossRef](#)]
48. Kessler, D.; McKee, R.J.; Hargrove, C.K.; Hincks, E.P.; Anderson, H.L. Muonic X rays and capture  $\gamma$  rays in  $^{89}\text{Y}$ . *Can. J. Phys.* **1970**, *48*, 3029–3037. [[CrossRef](#)]
49. Kessler, D.; Mes, H.; Thompson, A.C.; Anderson, H.L.; Dixit, M.S.; Hargrove, C.K.; McKee, R.J. Muonic x rays in lead isotopes. *Phys. Rev. C* **1975**, *11*, 1719. [[CrossRef](#)]
50. Anderson, H.L.; Hargrove, C.K.; Hincks, E.P.; McAndrew, J.D.; McKee, R.J.; Barton, R.D.; Kessler, D. Precise Measurement of the Muonic X Rays in the Lead Isotopes. *Phys. Rev.* **1969**, *187*, 1565–1596. [[CrossRef](#)]
51. IAEA. Live Chart of Nuclides. Available online: <https://www-nds.iaea.org/relnsd/vcharthtml/VChartHTML.html> (accessed on 11 January 2022).
52. Ninomiya, K.; Kubo, M.K.; Strasser, P.; Shinohara, A.; Tampo, M.; Kawamura, N.; Miyake, Y. Isotope Identification of Lead by Muon Induced X-ray and Gamma-ray Measurements. *JPS Conf. Proc.* **2018**, *21*, 011043. [[CrossRef](#)]
53. Hillier, A.; Ishida, K.; Seller, P.; Veale, M.C.; Wilson, M.D. Element Specific Imaging Using Muonic X-rays. *JPS Conf. Proc.* **2018**, *21*, 011042. [[CrossRef](#)]
54. Yabu, G.; Katsuragawa, M.; Tampo, M.; Hamada, K.; Harayama, A.; Miyake, Y.; Oshita, S.; Saito, S.; Sato, G.; Takahashi, T.; et al. Imaging of Muonic X-ray of Light Elements with a CdTe Double-Sided Strip Detector. *JPS Conf. Proc.* **2018**, *21*, 011044. [[CrossRef](#)]